International Journal of Mass Spectrometry 308 (2011) 175–180

Contents lists available at ScienceDirect

International Journal of Mass Spectrometry

journal homepage: www.elsevier.com/locate/ijms

The gas-phase *bis*-uranyl nitrate complex $[(UO_2)_2(NO_3)_5]^-$: Infrared spectrum and structure

Gary S. Groenewold[a,*], Michael J. van Stipdonk[b], Jos Oomens[c,e], Wibe A. de Jong[d], Michael E. McIlwain[a]

[a] *Idaho National Laboratory, 2151 North Blvd., Idaho Falls, ID 83402 USA*
[b] *Wichita State University, Department of Chemistry, 1845 Fairmont Ave, Wichita, KS, USA*
[c] *FOM Institute for Plasmaphysics, Nieuwegein, The Netherlands*
[d] *EMSL, Pacific Northwest National Laboratory, Richland, WA, USA*
[e] *van 't Hoff institute for Molecular Sciences, University of Amsterdam, Amsterdam, The Netherlands*

ARTICLE INFO

Article history:
Received 25 March 2011
Received in revised form 17 May 2011
Accepted 1 June 2011
Available online 30 June 2011

Keywords:
Infrared spectroscopy
Photodissociation
IRMPD
Density functional theory
Actinide complex
Uranium
Uranyl cluster
Free electron laser
FTMS

ABSTRACT

The infrared spectrum of the *bis*-uranyl nitrate complex $[(UO_2)_2(NO_3)_5]^-$ was measured in the gas phase using multiple photon dissociation (IRMPD). Intense absorptions corresponding to the nitrate symmetric and asymmetric vibrations, and the uranyl asymmetric vibration were observed. The nitrate ν_3 vibrations indicate the presence of nitrate in a bridging configuration bound to both uranyl cations, and probably two distinct pendant nitrates in the complex. The coordination environment of the nitrate ligands and the uranyl cations were compared to those in the *mono*-uranyl complex. Overall, the uranyl cation is more loosely coordinated in the *bis*-uranyl complex $[(UO_2)_2(NO_3)_5]^-$ compared to the *mono*-complex $[UO_2(NO_3)_3]^-$, as indicated by a higher O–U–O asymmetric stretching (ν_3) frequency. However, the pendant nitrate ligands are more strongly bound in the *bis*-complex than they are in the *mono*-uranyl complex, as indicated by the ν_3 frequencies of the pendant nitrate, which are split into nitrosyl and O–N–O vibrations as a result of bidentate coordination. These phenomena are consistent with lower electron density donation per uranyl by the nitrate bridging two uranyl centers compared to that of a pendant nitrate in the *mono*-uranyl complex. The lowest energy structure predicted by density functional theory (B3LYP functional) calculations was one in which the two uranyl molecules bridged by a single nitrate coordinated in a *bis*-bidentate fashion. Each uranyl molecule was coordinated by two pendant nitrate ligands. The corresponding vibrational spectrum was in excellent agreement with the IRMPD measurement, confirming the structural assignment.

1. Introduction

The structures of metal coordination complexes strongly influence their reactivity and disposition in the environment and in industrial processes. For example in uranium chemistry, structure and stability of coordination complexes involving the UO_2^{2+} (uranyl) cation control partition between aqueous and organic phases in metal separations of spent nuclear fuel [1–5]. Examining metal coordination complexes in the condensed phases is challenging because complexes are influenced not only by inner coordination sphere bonding, but also by the surrounding matrix, e.g. solvent molecules in solution or adsorptive sites on surfaces. These interactions make understanding the intrinsic chemistry of uranyl complexes challenging.

A powerful method for probing the intrinsic chemistry of metal species is to move them into the matrix-free environment of the gas phase, and then measure their infrared spectra. A variety of approaches have been used to get metal complexes into the gas phase, including laser vaporization [6–9] and particle bombardment [10], both of which have been used to investigate uranium species. A particularly efficient method for generating metal complexes in the gas phase is electrospray ionization [11–17]; when combined with trapped ion mass spectrometry and infrared multiple photon dissociation (IRMPD) this approach has enabled determination of the structures of many gas-phase ions, including a number of uranyl complexes [18–21]. IRMPD studies of gas-phase ions require an intense photon source, and a free electron laser such as that at the FELIX facility [22–27] has been used for studies of uranyl dication solvent complexes [28], ion-pair complexes [29,30], tris-anion complexes [30–32], and reduced uranyl (U(V)) complexes [33].

IRMPD experiments are performed in tandem with complementing density functional theory calculations (DFT) [34–36]. This approach simultaneously accomplishes two things: it facilitates

* Corresponding author. Tel.: +1 208 526 2803.
E-mail addresses: gary.groenewold@inl.gov, garygroenewold@gmail.com (G.S. Groenewold), michael.vanstipdonk@wsu.edu (M.J. van Stipdonk), joso@rijnh.nl (J. Oomens), bert.dejong@pnl.gov (W.A. de Jong).

1387-3806/$ – see front matter © 2011 Elsevier B.V. All rights reserved.
doi:10.1016/j.ijms.2011.06.002

interpretation of the measured vibrational frequencies, and it provides an evaluation of the performance of the DFT approaches. Computational modeling of actinide species is still at the frontier of computational science, and the IRMPD measurements provide frequency values that are not influenced by solvent interactions, and thus can be compared directly with the DFT results.

While the structures of uranyl coordination complexes investigated by IRMPD numbers about two dozen, no multi-uranyl clusters have yet been studied. These species are important because actinide clustering is the first step in formation of crystals and colloids. Prior IRMPD studies of Group II metal nitrate coordination clusters having the general formula $[M_2(NO_3)_5]^-$ produced broad absorption suggesting the existence of multiple competing structures resulting in overlapping vibrational bands [37,38]. In the present study, the IRMPD spectrum of $[(UO_2)_2(NO_3)_5]^-$ is measured and calculated using DFT, with careful comparisons with analogous coordination complexes and clusters.

2. Experimental

2.1. Material and methods

2.1.1. Generation of bis-uranyl clusters by ESI

Uranyl nitrate solutions were generated by dissolving $UO_2(NO_3)_2$ (Sigma–Aldrich, Milwaukee, WI, USA) in water such that the concentration was 2 mM. This solution was then mixed with methanol in a 1:1 ratio for electrospray. ESI experiments were conducted in the same fashion as described previously [31], but are briefly described here.

A commercial Z-spray electrospray ionization source (Micromass, Manchester, UK) oriented orthogonally to the sampling cone was used to produce ions sampled at atmospheric pressure by a sampling cone. The ESI source potential was −2.1 kV and the skimmer cone 100 V. Nitrogen gas at ambient temperature was used to desolvate the ESI spray droplets. ESI spray rates were maintained between 10 and 25 μl/min.

2.1.2. Fourier transform ion cyclotron resonance mass spectrometry (FT-ICR-MS)

Ions were accumulated in an external hexapole for about 5 s prior to being injected into the ICR cell. The subject anion complex was isolated for IRMPD study using a stored waveform inverse Fourier transform (SWIFT) pulse [39], which ejected all species except those having the desired mass.

2.1.3. Infrared multiple photon dissociation (IRMPD)

The infrared spectra of the *bis*-uranyl complex was collected by monitoring the efficiency of IRMPD as a function of photon energy [40]. In this experiment, isolated complexes were irradiated using two FELIX macropulses (40 mJ per macropulse, 5 μs pulse duration, FWHM bandwidth around 0.5% of central λ). When the laser frequency matches that of a normal vibrational mode of the gas-phase ion, energy is absorbed and subsequently distributed throughout the ion by intramolecular vibrational redistribution (IVR). The IVR process allows the energy of each photon to be "relaxed" prior to the absorption of the next, and thus allows promotion of the ion's internal energy to the dissociation threshold by multiple photon absorption [40]. The infrared spectra obtained using the IRMPD method presented here may produce spectra equivalent to those obtained using linear absorption techniques [24,27]. Two comparisons involving uranyl complexes substantiate this opinion: (a) IRMPD produced nitrate and uranyl frequencies for the gas-phase $[UO_2(NO_3)_3]^-$ complex [31] that were within 1–2 cm^{-1} of those measured for the ammonium salt of the same anion [41]; (b) IRMPD produced benzoate frequencies for the gas phase $[UO_2(C_6H_5CO_2)_3]^-$ complex [32] that were within one to 2 cm^{-1} of those measured for the sodium benzoate salt [42].

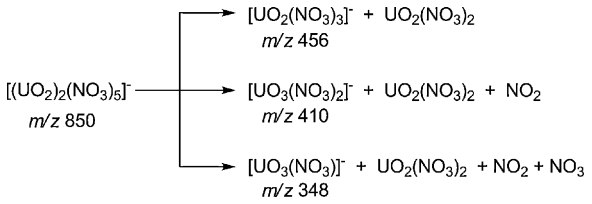

Scheme 1. Photodissociation reactions observed for the $[(UO_2)_2(NO_3)_5]^-$ complex.

To produce infrared spectra, the free electron laser was scanned in 0.01–0.04 μm increments between 6 and 11.5 μm, measuring product ions and un-dissociated precursor ions using the excite/detect sequence of the FT-ICR-MS [43,44] after each IRMPD step. The IRMPD yield was normalized to the summed fragment plus undissociated parent ion count, and corrected for variations in FELIX power over the spectral range. Three mass spectra were typically averaged for each FEL wavelength.

3. Density functional theory calculations

All calculations were performed using the NWChem software suite [45]. The optimized geometries, vibrational modes, and energetics were determined using the B3LYP exchange-correlation functional [46,47]. All reported energies in this paper include the zero-point energy correction at 0 K. The B3LYP frequencies were scaled by a factor of 0.98. For U the small core Stuttgart RECP and associated Stuttgart orbital basis sets [48–54] were used. For C, N, and O, the valence triple-ζ plus polarization (TZVP) DFT optimized basis sets were used [55]. In all cases, spherical basis sets were employed. Additional calculations were performed using the local density approximation (LDA) [56,57], with the same basis sets.

4. Results and discussion

4.1. IRMPD of the bis-uranyl complex $[(UO_2)_2(NO_3)_5]^-$

Electrospray of the uranyl nitrate solutions produced an abundant ion at *m/z* 850 that corresponded to the *bis*-uranyl complex $[(UO_2)_2(NO_3)_5]^-$. Isolation of this anion followed by irradiation using FELIX produced three salient fragment ions at *m/z* 456, 410, and 348 that correspond to the dissociation of the *bis*-uranyl complex (Scheme 1). The formation of $[UO_2(NO_3)_3]^-$ is by far the most abundant process, and consequently makes the largest contribution to the IRMPD spectrum.

The IRMPD spectrum was generated as the sum of all three dissociation channels (Fig. 1). The spectrum suggests a total of nine absorption bands (Table 1). The elimination of $UO_2(NO_3)_2$ to produce *m/z* 456 is by far the biggest contributor to the IRMPD

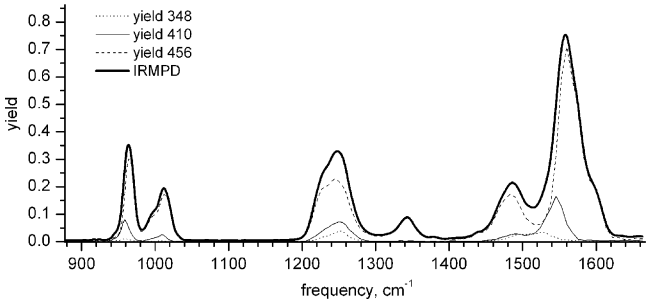

Fig. 1. IRMPD spectra generated from the sum of the dissociation channels (thick trace) and the three individual dissociation channels.

Table 1
Vibrational frequencies measured, and calculated (B3LYP) for $[(UO_2)_2(NO_3)_5]^-$ structure **a**. Calculated frequencies are scaled by 0.98, and intensities are scaled to 0.8 (the maximum yield in the IRMPD spectrum).

Frequency measured (cm^{-1})	Frequency calculated (cm^{-1})	Intensity calculated, arbitrary	Vibrational mode
964	976.76	0.382	Asymmetric O–U–O stretch (symmetric between uranium sites)
999 (shoulder), 1012	1024.92	0.075	Symmetric O–N–O stretch (asymmetric between pendant nitrates)
1233 (shoulder)	1237.32	0.173	Asymmetric O–N–O stretch (asymmetric between pendant nitrates, oxygen bonded to uranyl)
	1241.64	0.024	Asymmetric O–N–O stretch (asymmetric between pendant nitrates, oxygen bonded to uranyl)
1248	1255.21	0.257	Asymmetric O–N–O stretch (asymmetric between pendant nitrates, oxygen bonded to uranyl)
	1256.04	0.151	Asymmetric O–N–O stretch (asymmetric between pendant nitrates, oxygen bonded to uranyl)
1343	1344.28	0.168	Asymmetric O–N–O stretch (bridging nitrate bonded to both uranyls, oxygen in between two uranium atoms)
1486	1482.53	0.692	Asymmetric O–N–O stretch (bridging nitrate bonded to both uranyls, two pendant oxygen)
1558	1553.88	0.452	Asymmetric N=O stretch (asymmetric between pendant nitrates, pendant oxygen)
	1556.42	0.800	Asymmetric N=O stretch (asymmetric between pendant nitrates, pendant oxygen)
1594 (shoulder)	1566.83	0.145	Asymmetric N=O stretch (symmetric between pendant nitrates, pendant oxygen)
	1574.02	0.354	Asymmetric N=O stretch (symmetric between pendant nitrates, pendant oxygen)

spectrum. Sufficient energy was also deposited into the molecule to cause serial elimination of $(UO_2(NO_3)_2 + NO_2)$, generating a *bis*-nitrato-UO_3 anion at *m*/*z* 410 [31]. Elimination of NO_2 requires oxidation of some part of the remaining ion (composition is $[UO_3(NO_3)_2]^-$). This process does contribute to the IRMPD spectrum, and since it requires more energy, the major IR bands in the channel spectrum are slightly shifted to lower wavelength [58]. The fragment ion at *m*/*z* 348 arises from losses of $UO_2(NO_3)_2$, NO_2 and NO_3, and is observed in the mass spectra. Contributions of the *m*/*z* 410 and 348 dissociation channels to the summed IR spectrum are small, as shown in Figs. 1 and 2.

The peaks in the IRMPD spectrum of $[(UO_2)_2(NO_3)_5]^-$ can be assigned by comparison with IR spectra previously measured in the condensed phase, using matrix isolation spectroscopy, and using IRMPD. In the condensed phase, the infrared spectrum of nitrate is characterized by a single broadened absorption at about 1360–1400 cm^{-1} depending on the counter cation. However when a single metal nitrate molecule is isolated either in the gas phase or in a frozen matrix, the nitrate absorption is split into high and low frequency components. The high frequency component is interpreted in terms of the non-coordinating nitrosyl N=O moiety, while the low frequency component corresponds to the asymmetric stretch of the coordinated O–N–O moiety. In the IRMPD spectrum of $[(UO_2)_2(NO_3)_5]^-$ there are at least two sets of split nitrate absorptions, and probably a third.

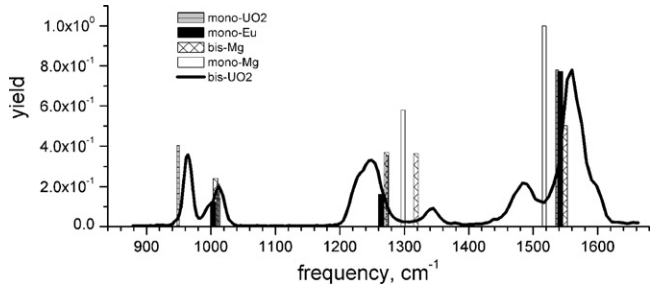

Fig. 2. Individual frequencies measured for comparable gas-phase nitrate complexes superimposed on the IRMPD spectrum of $[(UO_2)_2(NO_3)_5]^-$ (bis-UO_2 in the legend). *mono*-UO_2 represents $[UO_2(NO_3)_3]^-$ [31]. *mono*-Eu represents $[Eu(NO_3)_4]^-$ [31]. *bis*-Mg represents $[Mg_2(NO_3)_5]^-$ [38]. *mono*-Mg represents $[Mg(NO_3)_3]^-$ [37].

The most abundant peak in the IRMPD spectrum occurs at 1558 cm^{-1}, and corresponds to the nitrosyl stretch of a bound, pendant nitrate. The low frequency O–N–O absorption derived from this nitrate occurs at 1248 cm^{-1}. The strength of metal–nitrate binding can be correlated directly with the magnitude of the asymmetric nitrate splitting ($\Delta\nu_3$), which in this case was 310 cm^{-1}. There appear to be two other absorptions derived from pendant nitrate moieties that appear as shoulders on these two large peaks: the shoulders have frequencies at approximately 1594 cm^{-1} and 1233 cm^{-1} with a corresponding $\Delta\nu_3$ of 361 cm^{-1}. A third set of split nitrate frequencies are seen at 1486 and 1343 cm^{-1}, with a $\Delta\nu_3$ of only 143 cm^{-1}. The smaller magnitude of the $\Delta\nu_3$ in these frequencies is indicative of a much more symmetrical environment for this nitrate; one such environment would be a location in which the nitrate is bridging between the two uranyl metal centers.

The nitrate symmetric stretch is also activated in this spectrum, and it is observed at 1012 cm^{-1}. This peak has a lower frequency shoulder at ~999 cm^{-1} (compare its peak width with that of the uranyl asymmetric stretch at 964 cm^{-1}), which may correspond to another nitrate occupying a slightly different chemical environment. The peak at 964 cm^{-1} corresponds to the asymmetric O=U=O stretch.

Comparing the frequencies and splitting values for the nitrate absorptions with those measured for other complexes provides insight into the strength of binding of the nitrate. The structure of the *bis*-complex affects the binding strength of the pendant nitrates, as shown by a comparison of the nitrate absorptions for $[(UO_2)_2(NO_3)_5]^-$ with those for $[UO_2(NO_3)_3]^-$.

The frequencies and $\Delta\nu_3$ values for the pendant nitrate ligands indicate that they are more strongly bound in the *bis*-complex than they are in the *mono*-uranyl complex. The nitrosyl stretch for the pendant nitrates is shifted to higher frequency by 20 cm^{-1} in the *bis*-complex (main peak), and to an even larger value for the shoulder (57 cm^{-1} higher). The asymmetric O-N-O stretch involving principally the coordinating O atoms of the pendant nitrate ligands in the *bis*-complex is 25 cm^{-1} lower than in the analogous vibration in the *mono*-complex (40 cm^{-1} lower if the shoulder is considered). These shifts are summarized by the $\Delta\nu_3$ value for the

pendant nitrates, which is significantly increased from 264 cm^{-1} in the *mono*-complex to 310 in the *bis*-complex (361 measured between the shoulders). Stronger binding between the metal center and the two complexing-O atoms of the pendant nitrate will result in a strengthening of the nitrosyl bond, shifting it to higher frequency and resulting in a greater $\Delta\nu_3$ value. This is rationalized by the fact that even though the $UO_2(NO_3)_2$ moieties are in very similar environments in both the *bis*- and *mono*-complexes, the bridging nitrate in the *bis*-complex would be expected to donate less electron density to the metal center compared to the effect of a third pendant nitrate in the *mono*-complex. An alternative way to look at the effect is that there are 2.5 nitrate ligands per metal center in the *bis*-complex, compared to three in the *mono*-complex. The same effect can be seen in a comparison of the *bis*- and *mono*-Mg nitrate complexes: in the spectrum of the *bis*-Mg complex, the nitrosyl and O–N–O asymmetric frequencies are shifted to higher and lower values, respectively, compared to the *mono*-complex, and the $\Delta\nu_3$ value is thus increased for the *bis*-complex.[37,38]

The frequencies and $\Delta\nu_3$ values of the pendant nitrates in the *bis*-uranyl complex $[(UO_2)_2(NO_3)_5]^-$ indicate that these ligands are more strongly bound (and hence more structurally distorted) than in other metal complexes we have measured, including $[Eu(NO_3)_4]^-$, $[M(NO_3)_3]^-$ and $[M_2(NO_3)_5]^-$, where M = Group II cations.

In contrast, the bridging nitrate is in a much more symmetrical orientation, as indicated by the frequencies and $\Delta\nu_3$ values. Compared to the vibrations of the pendant nitrate ligands, both the nitrosyl and O–N–O asymmetric stretch of the bridging nitrate are shifted toward the single frequency measured for crystalline nitrate salts (~1400 cm^{-1}), in which nitrate assumes a symmetric trigonal planar geometry. The nitrosyl stretch of the bridging nitrate is much lower in frequency, and the O–N–O asymmetric stretch is higher. These values and the associated $\Delta\nu_3$ value (143 cm^{-1}) are well outside the envelopes for these vibrations as defined for pendant nitrate ligands by the spectra of the *mono*-metal complexes. The only comparison that is close is that seen in the IRMPD spectrum of the *bis*-Mg complex $[Mg_2(NO_3)_5]^-$, in which a resolved O–N–O asymmetric stretch for the bridging ligands is observed at 1318 cm^{-1}, a value 25 cm^{-1} lower than the analogous vibration in the *bis*-uranyl complex. This latter comparison indicates that the bridging nitrate ligands in the *bis*-uranyl complex exist in a more symmetrical geometry compared to the *bis*-Mg complex.

The nitrate symmetric ν_1 vibration at 1012 cm^{-1} is at the same value as the analogous vibration in the IRMPD spectrum of the *mono*-uranyl complex, which indicates that this vibration is not as sensitive to subtle changes in the binding environment of the coordination complexes as are the ν_3 nitrate vibrations. This conclusion is supported by the fact that the ν_3 vibration for the Eu and Group II nitrate anion complexes are within a few cm^{-1} of the values for the uranyl nitrate complexes. There does appear to be an unresolved peak on the low-frequency side of the ν_1 peak in the spectrum of the *bis*-complex, which may be derived from a nitrate in a significantly different environment.

The frequency of the asymmetric O–U–O vibration (UO_2 ν_3) was measured at 964 cm^{-1} in the spectrum of $[(UO_2)_2(NO_3)_5]^-$, which is 15 cm^{-1} higher than in the spectrum of $[UO_2(NO_3)_3]^-$. The UO_2 ν_3 vibration has been shown to be a remarkably sensitive indicator of the electron density provided by the ligands in the inner coordination sphere of the cation [28–30,32,33]. In this case, the higher frequency in the *bis*-uranyl complex indicates that overall the uranyl cation is less strongly coordinated than in the *mono*-uranyl complex. This conclusion is consistent with the earlier conclusion that the bridging nitrate is less strongly bound in the *bis*-complex compared to a third pendant nitrate in the *mono*-complex.

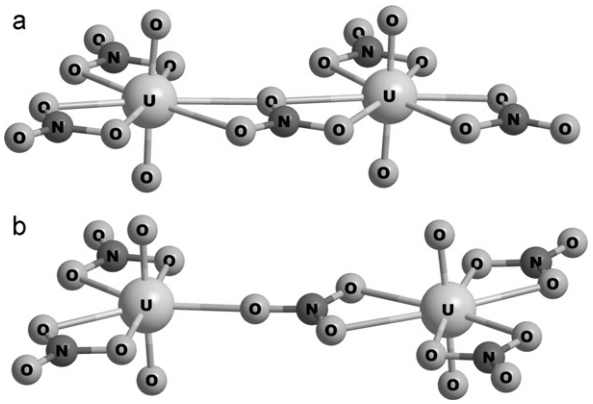

Fig. 3. Two energetically competitive structures for $[(UO_2)_2(NO_3)_5]^-$ structures calculated using the B3LYP functional.

4.2. DFT of the bis-uranyl complex

DFT calculations with theB3LYP functional located two minima (Fig. 3) that differed in energy by only 5 kcal/mol, with structure **a**, containing a *bis*-bidentate bridging nitrate being lower. The agreement of the IR spectrum calculated for structure **a** with the measured IRMPD spectrum was very good, while that calculated for structure **b** was poor, strongly suggesting that the *bis*-uranyl complex exists in the geometry of structure **a**. Specifically, the spectrum calculated for structure **b** contained a very intense band at 1423 cm^{-1} that corresponded to a symmetric mode of the bridging nitrate (Fig. S1). This band is completely absent in the IRMPD spectrum, enabling structure **a** to be identified between these two possibilities. Structure **a** is a natural precursor to building a trimer structure, requiring no re-organization but only addition of $UO_2(NO_3)_2$.

The agreement between the calculated and measured frequencies across the spectrum is very good (Table 1, a complete list of vibrational frequencies is found in Table S4). Four vibrational bands are assigned to nitrosyl stretches corresponding to two asymmetric modes and two different pendant nitrate ligands, from 1553 to 1574 cm^{-1}. When convoluted with a relatively large FWHM line shape function, both the maximum and shoulder of the IRMPD peak in this region are reproduced. The pendant nitrates are also responsible for four asymmetric O–N–O stretches that fall between 1237 and 1256 cm^{-1}, and again convolution of these peaks reproduces both the maximum and low frequency shoulder of the IRMPD peak. Finally the pendant nitrate ligands are responsible for symmetric stretches, the most significant of which is at 1025 cm^{-1}, which is about 13 cm^{-1} higher than the measurement. The low frequency shoulder observed in the experimental spectrum can be attributed to a lower intensity asymmetric combination of symmetric O–N–O stretches. The B3LYP calculations also very accurately reproduce the split O–N–O stretches of the bridging nitrate at 1343 and 1486 cm^{-1}, which strongly substantiates the structural assignment of this ligand. The last notable vibrational band in the IRMPD spectrum corresponds to the O–U–O asymmetric stretch, which was measured at 964 cm^{-1}, and here is B3LYP-calculated at 977 cm^{-1} (Table 2).

In prior experimental/theoretical studies we have employed the LDA functional to obtain the structure and vibrational frequencies of uranyl coordination complexes, and found that it was effective for predicting the UO_2 ν_3 stretching vibration, but was less accurate for the ligand vibrations [28]. LDA calculations performed for the $[(UO_2)_2(NO_3)_5]^-$ dimer also produced structure **a**, in agreement with the B3LYP results. In Fig. 4b (Table S6) the calculated vibrational frequencies are compared with the experimental results. In general the agreement between the measurement and calcula-

Table 2
$\Delta\nu_3$ values for nitrate ligands in the $[(UO_2)_2(NO_3)_5]^-$ complex compared with those measured for comparable gas-phase metal nitrate complexes.

Complex	Binding	$\Delta\nu_3$ (cm^{-1})	Refs.
bis, $[(UO_2)_2(NO_3)_5]^-$	Pendant	361	This work
bis, $[(UO_2)_2(NO_3)_5]^-$	Pendant	310	This work
bis, $[(UO_2)_2(NO_3)_5]^-$	Bridging	143	This work
mono, $[UO_2(NO_3)_3]^-$	Pendant	264	[26]
mono, $[UO_3(NO_3)_2]^-$	Pendant	248	[26]
mono, $[Eu(NO_3)_4]^-$	Pendant	278	[26]
mono, $[Mg(NO_3)_3]^-$	Pendant	219	[32]
mono, $[Ca(NO_3)_3]^-$	Pendant	208	[32]
mono, $[Sr(NO_3)_3]^-$	Pendant	200	[32]
mono, $[Ba(NO_3)_3]^-$	Pendant	198	[32]
bis, $[Mg_2(NO_3)_3]^-$	Pendant	254	[33]
bis, $[Ca_2(NO_3)_3]^-$	Pendant	234	[33]
bis, $[Sr_2(NO_3)_3]^-$	Pendant	220	[33]

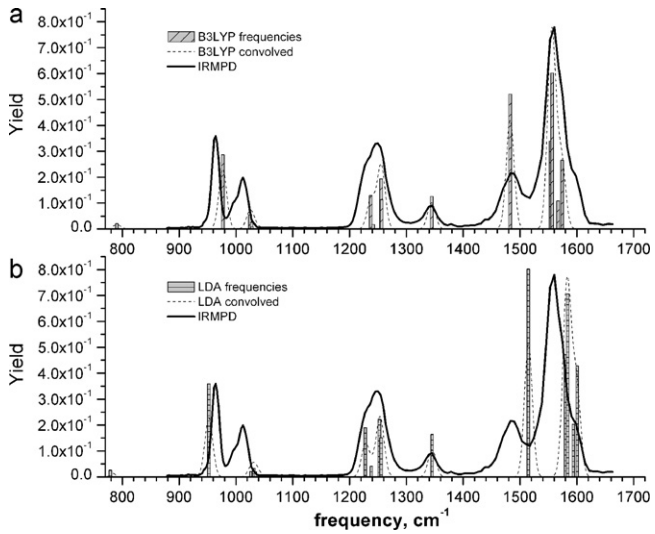

Fig. 4. (a) Convolved B3LYP-calculated spectrum (dashed line) with individual frequencies (columns) calculated for $[(UO_2)_2(NO_3)_5]^-$ structure **a**. (b) LDA-calculated spectrum and individual frequencies. The heavy line is the IRMPD spectrum in both a and b.

tion was good, especially for the mid-frequency ranges where the low-frequency components of the split nitrate O–N–O asymmetric stretches lie. The high-frequency modes of the split nitrate vibrations, and the symmetric O–N–O stretch of the pendant nitrates were slightly over-predicted (by about 20 cm^{-1}), whereas the frequency calculated for the asymmetric O–U–O stretch was about 10 cm^{-1} lower than the IRMPD spectrum (Fig. 5).

The agreement between the IRMPD measurement and the B3LYP spectrum strongly points to structure **a**, which is highly symmetrical, and indeed has three discrete nitrate environments. To enable differentiation, the nitrate ligands are described as either proximal or distal with respect to the U–O–U bridge (bond distances 2.692 Å). The two bridge-proximal nitrates are more tightly bound, with slightly shorter U–O bonds (~2.45 Å), whereas in contrast the two bridge-distal nitrates are slightly more loosely bound, and the nitrates are not symmetric, i.e., the two U-O bonds are not equivalent but instead have bond distances of ~2.462 and 2.474 Å. This results in a slightly stronger nitrosyl bond in the bridge-distal ligands compared to the analogous moieties in the bridge-proximal nitrates. The differing chemical environments of the bridge-proximal and bridge-distal nitrates are consistent with the broadened peaks assigned to the pendant nitrates in the IRMPD spectrum. The idea derived from the IR data that the bridging nitrate is more loosely attached to the metal centers is confirmed by the longer U–O distances, 2.692 and 2.607 Å. The more symmetric environment of this nitrate is consistent with smaller splitting of the asymmetric nitrate vibration.

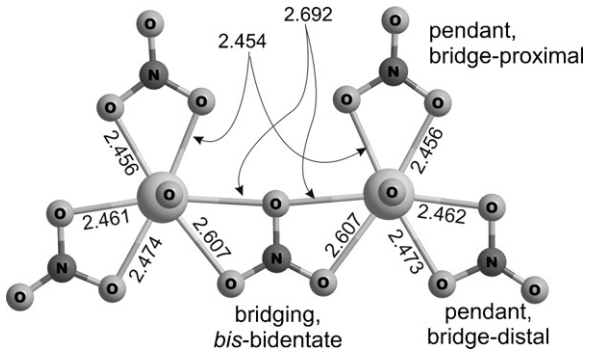

Fig. 5. Top view of the $[(UO_2)_2(NO_3)_5]^-$ complex structure **a**.

5. Conclusions

The combination of infrared multiple photon dissociation spectroscopy and density functional calculations show that in the absence of solvent, the *bis*-uranyl complex $[(UO_2)_2(NO_3)_5]^-$ adopts a highly symmetric structure in which two $UO_2(NO_3)_2$ molecules are bridged by a single nitrate. All five nitrate ligands in the complex are in the shared equatorial plane of the two uranyl molecules. The bridging nitrate exists in a *bis*-bidentate configuration with respect to the two uranyl metal centers, and is displaced from the U–U axis of the complex. The two pendant nitrate ligands on each uranyl have very similar, but unique chemical environments. The IRMPD spectrum of the gas-phase complex contained nitrate stretching modes split into high and low components corresponding to nitrosyl and O–N–O (bound to U) vibrations, respectively. The magnitude of the splitting of the stretching modes of the pendant nitrate ligands exceeds that of the monomeric anion[31] $[UO_2(NO_3)_3]^-$, indicating stronger bonding in the *bis*-complex. The nitrate stretching mode is also split for the bridging nitrate, but the magnitude of the splitting is much lower, consistent with a much more symmetric geometry of this ligand and generally weaker coordination to the uranyl metal centers. The frequency for the asymmetric O–U–O stretching vibration is also measured and indicates that the uranium metal center is less strongly coordinated in the $[(UO_2)_2(NO_3)_5]^-$ complex compared to the monomeric $[UO_2(NO_3)_3]^-$, a conclusion consistent with the presence of a shared (bridging) nitrate in the former complex.

Acknowledgments

Work by G.S. Groenewold, G.L. Gresham and M.E. McIlwain was supported by the U.S. Department of Energy, Assistant Secretary for Environmental Management, and the INL Laboratory Directed Research & Development Program under DOE Idaho Operations Office Contract DE-AC07-05ID14517. M.J. Van Stipdonk was supported through a grant from the U.S. National Science Foundation (NSF grant CAREER-0239800). J. Oomens was supported by the Nederlandse Organisatie voor Wetenschappelijk Onderzoek (NWO) and the Stichting Physica. The skillful assistance by the FELIX staff, in particular Dr. B. Redlich, is gratefully acknowledged. Construction and shipping of the FT-ICR-MS instrument was made possible through funding from the National High Field FT-ICR Facility (grant CHE-9909502) at the National High Magnetic Field Laboratory, Tallahassee, FL. A portion of W.A. de Jong's research was supported by the BES Heavy Element Chemistry program, Office of Basic Energy Sciences, U.S. Department of Energy, and performed using EMSL,

a national scientific user facility sponsored by the Department of Energy's Office of Biological and Environmental Research and located at Pacific Northwest National Laboratory.

Appendix A. Supplementary data

Supplementary data associated with this article can be found, in the online version, at doi:10.1016/j.ijms.2011.06.002.

References

[1] G. Choppin, Radiochim. Acta 92 (2004) 519.
[2] E.E. Sood, S.K. Patil, J. Radioanal. Nucl. Chem. 203 (1996) 547.
[3] A.P. Paiva, P. Malik, J. Radioanal. Nucl. Chem. 261 (2004) 485.
[4] J.N. Mathur, M.S. Murali, K.L. Nash, Solvent Extr. Ion Exch. 19 (2001) 357.
[5] W.W. Schultz, E.P. Horwitz, Sep. Sci. Technol. 23 (1988) 1191.
[6] T.M. Ayers, B.C. Westlake, D.V. Preda, L.T. Scott, M.A. Duncan, Organometallics 24 (2005) 4573.
[7] V. Goncharov, L.A. Kaledin, M.C. Heaven, J. Chem. Phys. 125 (2006) 133202–133211.
[8] J.M. Merritt, J. Han, M.C. Heaven, J. Chem. Phys. 128 (2008) 084304–84311.
[9] E.D. Pillai, K.S. Molek, M.A. Duncan, J. Chem. Phys. 405 (2005) 247.
[10] G.L. Gresham, A.K. Gianotto, P.d.B. Harrington, L. Cao, J.R. Scott, J.E. Olson, A.D. Appelhans, M.J. Van Stipdonk, G.S. Groenewold, J. Phys. Chem. A 107 (2003) 8530.
[11] G.S. Groenewold, Electrospray ionization of metal species, in: D. Beauchemin, D.E. Matthews (Eds.), Elemental and Isotope Ratio Mass Spectrometry, in: M.L. Gross, R.M. Caprioli (Eds.), The Encyclopedia of Mass Spectrometry, vol. 5, Elsevier, Amsterdam, 2010, p. 361.
[12] J.C. Traeger, Characterization of inorganic species in solution by ESI, in: D. Beauchemin, D.E. Matthews (Eds.), Elemental and Isotope Ratio Mass Spectrometry., in: M.L. Gross, R.M. Caprioli (Eds.), The Encyclopedia of Mass Spectrometry, vol. 5, Elsevier, Amsterdam, 2010, p. 369.
[13] V.B. Di Marco, G.G. Bombi, Mass Spectrom. Rev. 25 (2006) 347.
[14] L.C. Gatlin, F. Turecek, Electrospray ionization of inorganic and organometallic complexes, in: R.B. Cole (Ed.), Electrospray Ionization Mass Spectrometry; Fundamentals, Instrumentation, and Applications, John Wiley, New York, 1997, p. p. 527.
[15] M.J. Keith-Roach, Anal. Chim. Acta 678 (2010) 140.
[16] I.I. Stewart, Spectrochim. Acta, Part B 54 (1999) 1649.
[17] M.A. Duncan, Int. Rev. Phys. Chem. 22 (2003) 407.
[18] J.R. Eyler Mass, Spectrom. Rev. 28 (2009) 448.
[19] J. Lemaire, P. Boissel, M. Heninger, G. Mauclaire, G. Bellec, H. Mestdagh, A. Simon, S. Le Caer, J.M. Ortega, F. Glotin, P. Maitre, Phys. Rev. Lett. 89 (2002) 273002.
[20] N.C. Polfer, J. Oomens, Mass Spectrom. Rev. 28 (2009) 468.
[21] J.J. Valle, J.R. Eyler, J. Oomens, D.T. Moore, A.F.G. van der Meer, G. von Helden, G. Meijer, C.L. Hendrickson, A.G. Marshall, G.T. Blakney, Rev. Sci. Instrum. 76 (2005) 023103.
[22] J. Oomens, B.G. Sartakov, A.G.G.M. Tielens, G. Meijer, G. Von Helden, Astrophys. J. 500 (2001) L99.
[23] A. Fielicke, R. Mitric, G. Meijer, V. Bonacic-Koutecky, G. von Helden, J. Am. Chem. Soc. 125 (2003) 15716.
[24] J. Oomens, A.G.G.M. Tielens, B.G. Sartakov, G. Von Helden, G. Meijer, Astrophys. J. 591 (2003) 968.
[25] K. Asmis, G. Meijer, M. Brümmer, C. Kaposta, G. Santambrogio, L. Wöste, J. Sauer, J. Chem. Phys. 120 (2004) 6461.
[26] D.T. Moore, J. Oomens, J.R. Eyler, G. Meijer, G. von Helden, D.P. Ridge, J. Am. Chem. Soc. 126 (2004) 14726.
[27] J. Oomens, D.T. Moore, G. von Helden, G. Meijer, R.C. Dunbar, J. Am. Chem. Soc. 126 (2004) 724.
[28] G.S. Groenewold, A.K. Gianotto, K.C. Cossel, M.J. Van Stipdonk, D.T. Moore, N. Polfer, J. Oomens, W.A. de Jong, L. Visscher, J. Am. Chem. Soc. 107 (2006) 4802.
[29] G.S. Groenewold, A.K. Gianotto, M.E. McIlwain, M.J. Van Stipdonk, M. Kullman, D.T. Moore, N. Polfer, J. Oomens, I. Infante, L. Visscher, B. Siboulet, W.A. De Jong, J. Phys. Chem. A 112 (2008) 508.
[30] G.S. Groenewold, M.J. van Stipdonk, J. Oomens, W.A. de Jong, G.L. Gresham, M.E. McIlwain, Int. J. Mass Spectrom. 297 (2010) 67.
[31] G.S. Groenewold, J. Oomens, W.A. de Jong, G.L. Gresham, M.E. McIlwain, M.J. Van Stipdonk, Phys. Chem. Chem. Phys. 10 (2008) 1192.
[32] G.S. Groenewold, W.A. de Jong, J. Oomens, M.J. Van Stipdonk, J. Am. Soc. Mass Spectrom. 21 (2010) 719.
[33] G.S. Groenewold, M.J. van Stipdonk, W.A. de Jong, J. Oomens, G.L. Gresham, M.E. McIlwain, D. Gao, B. Siboulet, L. Visscher, M. Kullman, N. Polfer, Chem. Phys. Chem. 9 (2008) 1278.
[34] G.A. Shamov, G. Schreckenbach, T.N. Vo, Chem. Eur. J. 13 (2007) 4932.
[35] N. Kaltsoyannis, Chem. Soc. Rev. 32 (2003) 9.
[36] W.A. de Jong, E. Apra, T.L. Windus, J.A. Nichols, R.J. Harrison, K.E. Gutowski, D.A. Dixon, J. Phys. Chem. A 109 (2005) 11568.
[37] J. Oomens, L. Myers, R. Dain, C. Leavitt, V. Pham, G. Gresham, G. Groenewold, M. Van Stipdonk, Int. J. Mass Spectrom. 273 (2008) 24.
[38] C.M. Leavitt, J. Oomens, R.P. Dain, J. Steill, G.S. Groenewold, M.J. Van Stipdonk, J. Am. Soc. Mass Spectrom. 20 (2009) 772.
[39] A.G. Marshall, T.-C.L. Wang, T.L. Ricca, J. Am. Chem. Soc. 107 (1985) 7893.
[40] V.N. Bagratashivili, V.S. Letokov, A.A. Makarov, E.A. Ryabov, Mutiple Photon Infrared Laser Photophysics and Photochemistry, Harwood, Chur, Switzerland, 1985.
[41] M. Gal, P.L. Goggin, J. Mink, Spectrochim. Acta 48A (1992) 121.
[42] S.G. Lias, NIST Chemistry WebBook, United States Department of Commerce, National Institute of Standards and Technology, 2003, http://webbook.nist.gov/.
[43] A.G. Marshall, Acc. Chem. Res. 18 (1985) 316.
[44] A.G. Marshall, C.L. Hendrickson, G.S. Jackson, Mass Spectrom. Rev. 17 (1998) 1.
[45] M. Valiev, E.J. Bylaska, N. Govind, K. Kowalski, T.P. Straatsma, H.J.J. van Dam, D. Wang, J. Nieplocha, E. Apra, T.L. Windus, W.A. de Jong, Comput. Phys. Commun. 181 (2010) 1477.
[46] A.D. Becke, J. Chem. Phys. 98 (1993) 5648.
[47] C.T. Lee, W.T. Yang, R.G. Parr, Phys. Rev. B 37 (1988) 785.
[48] A. Bergner, M. Dolg, W. Kuchle, H. Stoll, H. Preuss, Mol. Phys. 80 (1993) 1431.
[49] M. Dolg, H. Stoll, H. Preuss, R.M. Pitzer, J. Phys. Chem. 97 (1993) 5852.
[50] P. Fuentealba, H. Preuss, H. Stoll, L. Vonszentpaly, Chem. Phys. Lett. 89 (1982) 418.
[51] P. Fuentealba, L. Vonszentpaly, H. Preuss, H. Stoll, J. Phys. B-At. Mol. Opt. Phys. 18 (1985) 1287.
[52] G. Igel-Mann, H. Stoll, H. Preuss, Mol. Phys. 65 (1988) 1321.
[53] W. Kuchle, M. Dolg, H. Stoll, H. Preuss, Mol. Phys. 74 (1991) 1245.
[54] W. Kuchle, M. Dolg, H. Stoll, H. Preuss, J. Chem. Phys. 100 (1994) 7535.
[55] N. Godbout, D.R. Salahub, J. Andzelm, E. Wimmer, Can. J. Chem. Rev. Can. Chim. 70 (1992) 560.
[56] J.C. Slater, Phys. Rev. Lett. 81 (1951) 385.
[57] S.J. Vosko, W. Wilk, M. Nusair, Can. J. Phys. 58 (1980) 1200.
[58] J. Oomens, D.T. Moore, G. Meijer, G. von Helden, Phys. Chem. Chem. Phys. 6 (2004) 710.